International Atomic Energy Agency

INDC(CCP)-222/L

INDC INTERNATIONAL NUCLEAR DATA COMMITTEE

TRANSLATION OF SELECTED PAPERS PUBLISHED IN NUCLEAR CONSTANTS, VOLUME 2(51), MOSCOW 1983

Translated by the IAEA

November 1984

IAEA NUCLEAR DATA SECTION, WAGRAMERSTRASSE 5, A-1400 VIENNA

INDC(CCP)-222/L

TRANSLATION OF SELECTED PAPERS PUBLISHED IN NUCLEAR CONSTANTS, VOLUME 2(51), MOSCOW 1983

Abstract

Translation of 5 papers from Nuclear Constants Volume 2(51) Moscow (1983). The original report was distributed as INDC(CCP)-207/G.

Translated by the IAEA

November 1984

Reproduced by the IAEA in Austria
November 1984

84-06219

Table of Contents

Translated from Russian

UDK 539.173.4

TESTING ^{239}Pu RESONANCE PARAMETERS IN THE ENERGY RANGE 4 TO 50 eV

V.A. Kon'shin, G.B. Morogovskij

In recent years detailed measurements of neutron transmission functions and of fission self-indication have been carried out for ^{239}Pu samples of various thicknesses [1], and these measurements have made it possible to test the resonance parameters of ^{239}Pu. This task is especially urgent in view of the lack of reliable microscopic data for ^{239}Pu on transmission in the resonance region, which has meant that evaluated resonance parameters [2] could be obtained only on the basis of total cross-section data that are nearly 20 years old [3,4] and for which the experimental resolution function is not accurately known. The direct use in the analysis of experimental data on transmission for a given set of thicknesses can be expected to reduce the uncertainties arising from imprecise knowledge of the resolution function (only with very narrow thicknesses can the resolution function for the total cross-section be obtained from the resolution function for transmission) and from other possible systematic errors, e.g. inaccurately defined sample thicknesses.

As our starting point we selected a system of evaluated resonance parameters [2] which permits the available experimental neutron cross-section data to be described unequivocally in the resonance region. With the aid of this system of parameters we tried to describe as well as possible the detailed behaviour of the transmission and fission self-indication functions for five samples of ^{239}Pu [1], varying the initial resonance parameters as required.

Van'kov and co-workers [1] measured neutron transmission functions over path lengths of around 1000 and 250 m and fission self-indication over a path length of approximately 78 m. The geometry of the experiment is such that neutron scattering into the detector can be disregarded. Transmission measurements were carried out for five samples varying in thickness from 0.00862 nuclei/b to 0.1294 nuclei/b over the path length of 1000 m (1st series) and for one sample having a thickness of about 0.03 nuclei/b over the path length of 250 m (2nd series) with much better resolution than in the first

series. Fission self-indication was measured for three samples ranging from 0.00217 to 0.0173 nuclei/b. All measurements were made at room temperature; the amount of ^{240}Pu impurity in the samples was determined from the shape of the experimental curve.

The resonance parameters were tested in three stages. During the first stage the transmission functions for the series of five samples (average path length 1000 $\pm$ 5 m) were treated simultaneously. The exact path lengths and time lags were calculated for each sample on the basis of the energy scale adopted, referenced to the most clearly defined resonances. For this purpose we took the energy scale of Ribon and Le Cog [5], which is practically the same as the experimental scale [6].

The parameters Γ_n^o and $\Gamma_a = \Gamma_f + \Gamma_\gamma$ were calculated by means of the Breit-Wigner formalism. For each resonance calculated, the contribution from 50 neighbouring resonances (25 to the right and 25 to the left of the resonance of interest) was taken into account. This made it possible to take into account the contributions to the last resonance treated (at 49.7 eV) from the broad resonances at 96.49 and 100.25 eV; the contribution from the resonance at 100.25 eV amounted to 0.07 b, which indicates that an adequate number of resonances were considered. Moreover, 13 resonances of ^{240}Pu, which were also considered in the treatment, contribute to the region of interest. The resonance parameters of ^{240}Pu are taken from Ref. [7]. The parameters Γ_n^o and Γ_a for each resonance were varied within certain limits in order to get an optimum description of the curve behaviour for all five samples:

$$T_t(E) = \int_{\Delta E} \exp\left[-x\sigma_t(E')\right] R(E,E')dE', \qquad (1)$$

where x is the thickness of the sample; $\sigma_t(E')$ is the total cross-section at a given energy point (the temperature dependence is normally taken into account via ψ and χ functions), which depends on the variable parameters; and R(E,E') is the experimental resolution function. The value of the potential scattering cross-section was taken as 10.35 b [2], which agrees with the data in Ref. [8] (10.30 $\pm$ 0.15 b) and makes it possible to reconcile the scattering cross-section at the thermal point (7.4 b) with the estimate from Ref. [9] (7.2 $\pm$ 1.4 b) when parametrizing the cross-sections in the thermal region.

The initial values of the parameters are given in Table 1, together with the quantities $g\Gamma_n^o$ and Γ_a, obtained after first stage (1st series) fitting. During the second stage, the parameters of the first series were used as base data to describe the shape of the $T_t(E)$ curve for a sample having a thickness of 0.03019 nuclei/b with a path length of 250 m, measured separately with much better resolution than in the preceding series. The authors did not manage to get into the region above 50 eV because even at this energy level the distance between the experimental points is of the order of a full resonance width (0.2-0.3 eV). The resolution function in this experiment had a more complex form, and the computation time was thereby substantially increased. The system of parameters fitted for the description of the $T_t(E)$ curve in this sample also appears in Table 1 (2nd series). Subsequently, calculations of the $T_t(E)$ curve for the five samples of the first series were carried out using the parameters from series 2 in order to clarify which system of parameters best reproduces the transmissions for these five samples. We shall discuss the need for this procedure later. The calculations revealed that a combination of the parameters of both series (series 3 in Table 1) gives the best results.

Let us now consider some methodological questions arising from the solution of this problem:

1. It turned out to be impossible to carry out a combined evaluation of series 1 and 2 because of the large quantity of experimental information, so the experiments were processed separately.

2. The problem is typical of those requiring the minimization of a function of certain variables:

$$T_m = \sum_{k=1}^{n} \sum_{i=1}^{N} \frac{T_{eks_{k,i}} - T_{calc_{k,i}}}{\Delta T_{eks_{k,i}}} \longrightarrow min \ , \qquad (2)$$

where n is the number of samples and N is the number of experimental points. It turned out that the function in question has local minima in the region of each resonance (in the regions where changes in Γ_n^o and Γ_a occur), as a result of which it was not possible to utilize the usual methods of finding the function's minimum (gradient methods etc.). The problem was solved in the following manner: domains of change were established for each of the parameters, and T_m was computed for each pair of parameters; the pairs were

set up in such a way that each value of one parameter was correlated in turn with all the values of the other. The "best" pair of parameters, Γ_n^o and Γ_a, corresponded to the minimum value of T_m found in this manner. The certainty with which the overall minimum is found depends on the size of the parameter change steps, but if they are kept small enough the increase in computation time becomes a more significant factor than the accuracy of the parameters thereby obtained. Although the minimum ascertained may well not be an overall minimum, it is nevertheless generally "deeper" than the minima yielded by the gradient and other methods. Now it will be understood that treating series 1 and 2 separately may result in different values for parameters of one and the same resonance and, moreover, the resonance parameters of series 2 may describe the resonances of series 1 better than the actual series 1 parameters (deeper local minima are achieved in series 2).

Thus, after completing the first and second stages we have a set of resonance parameters $\{\Gamma_{n_i}^o, \Gamma_{a_i}\}$, which provide an optimum description of the experimental data indicated above.

Let us proceed now to the third stage. Since the fission self-indication function takes the form

$$T_f(E) = \frac{\int_{\Delta E} \sigma_f(E') \exp\left[-x\sigma_t(E')\right] R(E')\,dE'}{\int_{\Delta E} \sigma_f(E') R(E')\,dE'}, \qquad (3)$$

where $\sigma_f(E')$ is the fission cross-section at point E' and the other quantities have the same meaning as in expression (1), let us endeavour to solve the problem of finding the parameters Γ_f and Γ_γ for all the resonances under consideration. In fact, the parameters Γ_n^o and $\Gamma_a = \Gamma_f + \Gamma_\gamma$ have already been obtained, and the spins and resonance energies are also known [2]. If we now fix Γ_n^o and Γ_a and vary Γ_f in such a way that the condition $\Gamma_a = \Gamma_f + \Gamma_\gamma$ is fulfilled, i.e. by using only those values of Γ_f which do not take Γ_γ beyond some reasonable interval (see below), then values for Γ_f can be found for which condition (2) is fulfilled. This would automatically mean that the values of Γ_γ corresponding to them are likewise optimal. Thus this problem does not, in essence, differ from the one which was solved above. Let us now consider in detail how to treat the algorithm shown above.

We had at our disposal $T_f(E)$ values measured on three samples with thicknesses ranging from 0.00217 nuclei/b to 0.0173 nuclei/b; the resolution function had the same form as in series 2, and the resolution corresponded approximately to that in series 1. The resonance energies and spins were taken from Ref. [2]; Γ_n^o and Γ_a were taken from Table 1 (series 3) and fixed. Furthermore, given the physical meaning of the quantities Γ_f and Γ_γ, the following limitations were imposed on them:

(a) $\Gamma_f \geq 0.1 \times 10^{-2}$ eV; (b) 0.029 eV $\leq \Gamma_\gamma \leq$ 0.061 eV.

By varying Γ_f within the limits imposed by these conditions and requiring the fulfilment of condition (2), we expected to obtain more precise values of Γ_f and Γ_γ in the energy region indicated above and thereby to close our system of resonance parameters. It turned out, however, that $T_f(E)$ is not very responsive to changes in the value of Γ_f within the limits imposed by conditions (a) and (b). Table 2 shows calculations of $T_f(E)$ at experimental energy points very close to the peaks of the corresponding resonances for the various optimal values of Γ_f obtained by fitting.

The $\Gamma_{f\ init.}$ in Table 2 are values of Γ_f obtained from Γ_a (cf. series 3, Table 1) on the assumption that Γ_γ = 0.04 eV (except for those cases where the value of Γ_γ is in brackets); $\Gamma_{f\ init.}$ are calculated values of fission self-indication for each of the three samples at a given value of $\Gamma_{f\ init.}$; Γ_{f1} are values of Γ_f obtained by fitting to the experimental data, subject to the condition that the formula for calculating errors in the experimental data has the same form as in series 2. The self-indication values which correspond to these Γ_f are shown in column Γ_{f1}. The notation "max" against Γ_f denotes that the maximum possible value of Γ_f was reached if conditions (a) and (b) are taken as the starting point; the notation "mid" denotes that Γ_f is within the resolved interval. The Γ_{f2} were obtained by fitting subject to the condition that the error calculation formula has the form $\sim I/\sigma_t$, where σ_t is the total cross-section in Breit-Wigner form without allowance for Doppler broadening; this definition of the error means that the experimental points located closer to the resonance peak have the greatest weight, in contrast to the previous formula, where greater weight was attributed to points in the interresonance region.

These two methods of specifying the experimental errors would have been expected to give substantially different fitted values of Γ_f in view of the fact that the $T_f(E)$ data used have a very broad scatter in the interresonance region. It can be seen from Table 2 that this is indeed what happened. The notation "min" indicates that the fitting resulted in the smallest possible value of Γ_f. The values of T_f which correspond to these "min" values are shown in the T_{f2} column. An analysis of Table 2 reveals that the greatest possible changes in Γ_f do not effectively alter the values of T_f. This holds true for all resonances except two: those at 41.42 and 44.48 eV, which have large values of Γ_n^o compared with the other resonances. The two methods of specifying the experimental errors led to values of Γ_f for the corresponding resonances which were at opposite ends of the interval of allowed changes: the maximum values of Γ_f were given by the first method owing to the large scatter of T_f in the interresonance region; the minimum values resulted from the second method, except for those cases where there was a very small number of experimental points in the resonance region (for example at 49.71 eV) and where the resonance does not in effect emerge from the shape of the curve (for example at 11.5 eV).

It is thus evident that the experimental data on fission self-indication do not permit us to ascertain or test the values of the fission widths owing to the very low sensitivity of T_f to changes in the broad limits of Γ_f. However, using transmissions measured for various thicknesses we can obtain the resonance parameters Γ_n^o and Γ_a by the form method, where the effect of insufficiently precise measurement of the resonance peaks is not so telling. We may conclude that the experimental data of Van'kov and co-workers [1] do not contradict the available microscopic data for σ_t and enable us to obtain more accurate values of $g\Gamma_n$ for ^{239}Pu in the energy region below 50 eV. The currently available resonance parameters could be rendered very much more precise if experiments were carried out utilizing large sets of sample thicknesses with cooling and with good resolution for the various fissile nuclei.

REFERENCES

[1] VAN'KOV, A.A., GRIGOR'EV, Yu.V., UKRAINTSEV, B.F. et al., An experimental study of resonance self-shielding of the total cross-section and fission cross-section for ^{239}Pu, Voprosy atomnoj nauki i tekhniki (Questions of atomic science and technology) Nuclear Constants Series No. 2(37) (1980) 44–50.

[2] ANTSIPOV, G.V., BACHANOVICH, L.A., ZHARKOV, V.F. et al., Evaluation of nuclear data for ^{239}Pu, Part I: The resolved resonance region, 10^{-5}–660 eV, ITMO Preprint, Byelorussian Academy of Sciences, Minsk (1981) 1–48.

[3] DERRIEN, H., BLONS, G., EGGERMAN, C. et al., Sections efficaces total et de fission du ^{239}Pu. In: Proc. IAEA Conf. on Nuclear Data for Reactors (Paris, 1966). Vienna, IAEA, 1967, v. 2, p. 195–219.

[4] BOLLINGER, L.M., COTE, R.E., THOMAS, G.E., Low-energy total and fission cross-section measurements of ^{239}Pu. In: Proc. of the Intern. Conf. on Peaceful Uses of Atomic Energy. Geneva, 1958, v. 15, p. 127–135.

[5] RIBON, P., LE COG, G., Evaluation des Donnees Neutroniques de ^{239}Pu. CEA-N-1484. France, Saclay, 1971.

[6] GWIN, R., WESTON, L.W., DE SAUSSUVE, G. et al., Simultaneous measurement of the neutron fission and absorption cross-sections of ^{239}Pu over the energy region 0.02 eV to 30 keV. Nucl. Sci. and Engng, 1971, v. 45, p. 25–36.

[7] ANTSIPOV, G.V., KON'SHIN, V.A., SUCHOVITSKIJ, E.Sh., Nuclear constants for plutonium isotopes, Minsk (1981).

[8] UTTLEY, C.A., Neutron total cross-section measurements. Progress Report AERE-PR/N, 1967, p. 11; EANDC(UK)-35B, 1964.

[9] LEMMEL, H.D., The third IAEA evaluation of the 2200 m/s and 20°C Maxwellian neutron data for ^{233}U, ^{235}U, ^{239}Pu, ^{241}Pu. In: Proc. of the Conf. on Nucl. Cross-Sections and Technology. Washington, 1975, NB5, Spec. Public. 425, v. 1, p. 286–292.

This article was submitted on 4 February 1983.

Comparison of resonance parameters in the different series

Table 1

E_z	$g\Gamma_n$ init.	Γ_a init.	$g\Gamma_n$ (s.1)	Γ_a (s.1)	$g\Gamma_n$ (s.2)	Γ_a (s.2)	$g\Gamma_n$ (s.3)	Γ_a (s.3)	$\Delta g\Gamma_n$, %	$\Delta\Gamma_a$, %	Notes
5,9	$4,7\cdot10^{-3}$	3,3023	$4,7\cdot10^{-3}$	3,3023	$4,7\cdot10^{-3}$	3,3023	$4,7\cdot10^{-3}$	3,3023	0	0	Init.
7,82	$5,7351\cdot10^{-4}$	$8,7\cdot10^{-2}$	$5,4413\cdot10^{-4}$	$8,4097\cdot10^{-2}$	$6,195\cdot10^{-4}$	$7,8788\cdot10^{-2}$	$5,4413\cdot10^{-2}$	$8,4097\cdot10^{-2}$	5,12	3,34	I
10,93	$1,3239\cdot10^{-3}$	$1,988\cdot10^{-1}$	$1,1969\cdot10^{-3}$	$1,6683\cdot10^{-1}$	$1,2664\cdot10^{-3}$	$1,4915\cdot10^{-1}$	$1,1969\cdot10^{-3}$	$1,6683\cdot10^{-1}$	9,59	16,08	I
11,5	$4,2527\cdot10^{-5}$	$5,16\cdot10^{-2}$	$5,896\cdot10^{-5}$	$1,5693\cdot10^{-1}$	$4,8727\cdot10^{-5}$	$1,5693\cdot10^{-1}$	$4,8727\cdot10^{-5}$	$1,5693\cdot10^{-1}$	-14,58	-204,13	2
11,89	$6,6947\cdot10^{-4}$	$7,6\cdot10^{-2}$	$5,6684\cdot10^{-4}$	$6,4517\cdot10^{-2}$	$5,7916\cdot10^{-4}$	$5,8065\cdot10^{-2}$	$5,7916\cdot10^{-4}$	$5,8065\cdot10^{-2}$	13,49	23,60	2
14,31	$4,3221\cdot10^{-4}$	$1,01\cdot10^{-1}$	$7,181\cdot10^{-4}$	$1,0128\cdot10^{-1}$	$1,0191\cdot10^{-3}$	$9,9652\cdot10^{-2}$	$7,181\cdot10^{-4}$	$1,0128\cdot10^{-1}$	-66,15	-0,28	I
14,68	$1,4198\cdot10^{-3}$	$6,8\cdot10^{-2}$	$1,4235\cdot10^{-3}$	$6,3153\cdot10^{-2}$	$2,0783\cdot10^{-3}$	$6,1735\cdot10^{-2}$	$1,4235\cdot10^{-3}$	$6,3153\cdot10^{-2}$	-0,26	7,13	I
15,46	$4,6707\cdot10^{-4}$	$6,989\cdot10^{-1}$	$4,6677\cdot10^{-4}$	$6,989\cdot10^{-1}$	$5,3288\cdot10^{-4}$	$6,5965\cdot10^{-1}$	$4,6677\cdot10^{-4}$	$6,989\cdot10^{-1}$	0,06	0	I
17,66	$1,2249\cdot10^{-3}$	$7,3\cdot10^{-2}$	$1,2228\cdot10^{-3}$	$7,3\cdot10^{-2}$	$1,4921\cdot10^{-3}$	$6,8818\cdot10^{-2}$	$1,2228\cdot10^{-3}$	$7,3\cdot10^{-2}$	0,17	0	I
22,29	$1,8573\cdot10^{-3}$	$1,06\cdot10^{-1}$	$2,0272\cdot10^{-3}$	$9,5687\cdot10^{-2}$	$2,2315\cdot10^{-3}$	$8,6444\cdot10^{-2}$	$2,0272\cdot10^{-3}$	$9,5687\cdot10^{-2}$	-9,15	9,73	I
23,94	$6,386\cdot10^{-5}$	$7,0\cdot10^{-2}$	$6,9454\cdot10^{-5}$	$6,3603\cdot10^{-2}$	$6,2508\cdot10^{-5}$	$5,7387\cdot10^{-2}$	$6,2508\cdot10^{-5}$	$5,7387\cdot10^{-2}$	2,12	18,02	2
26,24	$8,9929\cdot10^{-4}$	$8,2002\cdot10^{-2}$	$1,1277\cdot10^{-3}$	$8,5466\cdot10^{-2}$	$1,2406\cdot10^{-3}$	$7,7188\cdot10^{-2}$	$1,1277\cdot10^{-3}$	$8,5466\cdot10^{-2}$	-25,4	-4,22	I
27,24	$1,0735\cdot10^{-4}$	$4,2\cdot10^{-2}$	$1,0209\cdot10^{-4}$	$3,6053\cdot10^{-2}$	$9,1883\cdot10^{-2}$	$3,2494\cdot10^{-5}$	$9,1883\cdot10^{-5}$	$3,2494\cdot10^{-2}$	14,41	22,63	2
32,31	$1,8747\cdot10^{-4}$	$1,51\cdot10^{-1}$	$1,877\cdot10^{-4}$	$1,51\cdot10^{-1}$	$1,7645\cdot10^{-4}$	$1,3671\cdot10^{-1}$	$1,7645\cdot10^{-4}$	$1,3671\cdot10^{-1}$	5,88	9,46	2
34,6	$9,16\cdot10^{-6}$	$9,1\cdot10^{-2}$	$9,16\cdot10^{-6}$	$9,1\cdot10^{-2}$	$8,244\cdot10^{-6}$	$8,2195\cdot10^{-2}$	$8,244\cdot10^{-6}$	$8,2195\cdot10^{-2}$	10,0	9,68	2
35,5	$2,0441\cdot10^{-4}$	$4,7\cdot10^{-2}$	$2,0458\cdot10^{-4}$	$4,7\cdot10^{-2}$	$1,8413\cdot10^{-4}$	$4,2379\cdot10^{-2}$	$1,8413\cdot10^{-4}$	$4,2379\cdot10^{-2}$	9,92	9,83	2
41,42	$3,1786\cdot10^{-3}$	$4,8\cdot10^{-2}$	$3,2605\cdot10^{-3}$	$5,3453\cdot10^{-2}$	$2,9343\cdot10^{-3}$	$4,8006\cdot10^{-2}$	$2,9343\cdot10^{-3}$	$4,8006\cdot10^{-2}$	7,69	-0,01	2
41,66	$1,1150\cdot10^{-3}$	$1,04\cdot10^{-1}$	$9,3891\cdot10^{-4}$	$8,7968\cdot10^{-2}$	$9,5769\cdot10^{-4}$	$7,8895\cdot10^{-2}$	$9,5769\cdot10^{-4}$	$7,8895\cdot10^{-2}$	14,11	24,14	2
44,48	$4,7088\cdot10^{-3}$	$5,2\cdot10^{-2}$	$4,0079\cdot10^{-3}$	$3,9964\cdot10^{-2}$	$4,5706\cdot10^{-3}$	$3,7626\cdot10^{-2}$	$4,0079\cdot10^{-3}$	$3,9964\cdot10^{-2}$	14,88	23,15	I
47,6	$1,4101\cdot10^{-3}$	$3,06\cdot10^{-1}$	$1,2087\cdot10^{-3}$	$2,3284\cdot10^{-1}$	$1,3299\cdot10^{-3}$	$2,1149\cdot10^{-1}$	$1,2087\cdot10^{-3}$	$2,3284\cdot10^{-1}$	14,28	23,91	I
49,71	$1,0143\cdot10^{-3}$	$7,98\cdot10^{-1}$	$9,2004\cdot10^{-4}$	$8,9682\cdot10^{-1}$	$1,2699\cdot10^{-3}$	$9,2145\cdot10^{-1}$	$9,2004\cdot10^{-4}$	$8,9682\cdot10^{-1}$	9,29	-12,38	I

Values of the quantities Γ_f and T_f

Table 2

E_z	Γ_f init.	T_f init.	Γ_{f_1}	T_{f_1}	Γ_{f_2}	T_{f_2}
5,9	$0,3259 \cdot 10^{-1}$ ($\Gamma_f = 0,0433$)	0,958429 0,84I2I2 0,707I03	$0,32573 \cdot 10^{-1}$ mid ($\Gamma_f = 0,045$)	0,95843 0,84I2I 0,707I0	$0,32493 \cdot 10^{-1}$ mid ($\Gamma_f = 0,053$)	0,95852 0,84I53 0,70764
7,82	$0,44097 \cdot 10^{-1}$	$0,549949 \cdot 10^{-1}$ $0,46I757 \cdot 10^{-3}$ $0,I66802 \cdot 10^{-2}$	$0,55097 \cdot 10^{-1}$ max	$0,54994 \cdot 10^{-1}$ $0,46I52 \cdot 10^{-3}$ $0,I6658 \cdot 10^{-2}$	$0,23097 \cdot 10^{-1}$ min	$0,54964 \cdot 10^{-1}$ $0,46I86 \cdot 10^{-3}$ $0,I67II \cdot 10^{-2}$
I0,93	0,I2683	0,I0I326 $0,708I35 \cdot 10^{-4}$ $0,I7588 \cdot 10^{-1}$	0,I3783 max	0,I0I33 $0,708I4 \cdot 10^{-4}$ $0,I7589 \cdot 10^{-1}$	0,I0583 min	0,I0I33 $0,708I8 \cdot 10^{-4}$ $0,I759I \cdot 10^{-1}$
II,50	0,II693	0,769656 0,349I54 0,I28638	0,I2793 max	0,76973 0,3493I 0,I287I	0,I2793 max	0,76952 0,34883 0,I2850
II,89	$0,I8065 \cdot 10^{-1}$	0,244768 $0,94I047 \cdot 10^{-2}$ $0,232773 \cdot 10^{-4}$	$0,29065 \cdot 10^{-1}$ max	0,24379 $0,92677 \cdot 10^{-2}$ $0,22959 \cdot 10^{-4}$	$0,I \cdot 10^{-2}$ min	0,26350 $0,II995 \cdot 10^{-1}$ $0,8I023 \cdot 10^{-4}$
I4,3I	$0,6I28 \cdot 10^{-1}$	0,I7I693 $0,25I627 \cdot 10^{-2}$ $0,I9896 \cdot 10^{-5}$	$0,7228 \cdot 10^{-1}$ max	0,I7I73 $0,25I56 \cdot 10^{-2}$ $0,I992 \cdot 10^{-5}$	$0,4028 \cdot 10^{-1}$ min	0,I6687 $0,23404 \cdot 10^{-2}$ $0,I3645 \cdot 10^{-5}$
I4,68	$0,23I53 \cdot 10^{-1}$	$0,23II6I \cdot 10^{-1}$ $0,526I77 \cdot 10^{-5}$ $0,2726I \cdot 10^{-3}$	$0,34I53 \cdot 10^{-1}$ max	0,23074 · I0 $0,5I524 \cdot 10^{-5}$ $0,26906 \cdot 10^{-8}$	$0,2I53 \cdot 10^{-2}$ min	$0,23828 \cdot 10^{-1}$ $0,733II \cdot 10^{-5}$ $0,3465I \cdot 10^{-8}$
I5,46	0,6489 ($\Gamma_f = 0,05$)	0,747786 0,3I475 $0,98756 \cdot 10^{-1}$	0,6699 max	0,74779 0,3I475 $0,98757 \cdot 10^{-1}$	0,6699 max	0,74779 0,3I475 $0,98756 \cdot 10^{-1}$
I7,66	$0,3240 \cdot 10^{-1}$	0,I27753 $0,26804 \cdot 10^{-3}$ $0,6I7I67 \cdot 10^{-3}$	$0,440 \cdot 10^{-1}$ max	0,I2772 $0,26775 \cdot 10^{-3}$ $0,6I329 \cdot 10^{-3}$	$0,I20 \cdot 10^{-1}$ min	0,I2799 $0,26989 \cdot 10^{-3}$ $0,64I8I \cdot 10^{-3}$
22,29	$0,55687 \cdot 10^{-1}$	$0,849I06 \cdot 10^{-1}$ $0,6I2462 \cdot 10^{-3}$ $0,II5982 \cdot 10^{-3}$	$0,66687 \cdot 10^{-1}$ max	$0,84905 \cdot 10^{-1}$ $0,6I223 \cdot 10^{-3}$ $0,II590 \cdot 10^{-3}$	$0,34687 \cdot 10^{-2}$ min	$0,8493I \cdot 10^{-1}$ $0,6I334 \cdot 10^{-3}$ $0,II630 \cdot 10^{-3}$

Table 2 (continued)

E_z	Γ_f init.	T_f init.	Γ_{f_1}	T_{f_1}	Γ_{f_2}	T_{f_2}
23,94	$0,17387 \cdot 10^{-1}$	0,900965 0,663048 0,400569	$0,28387 \cdot 10^{-1}$ max	0,89990 0,65972 0,39821	$0,1 \cdot 10^{-2}$ min	0,91490 0,70855 0,42387
26,24	$0,45466 \cdot 10^{-1}$	0,354078 $0,241406 \cdot 10^{-1}$ $0,195802 \cdot 10^{-2}$	$0,54466 \cdot 10^{-1}$ max	0,35406 $0,24128 \cdot 10^{-1}$ $0,19552 \cdot 10^{-2}$	$0,24466 \cdot 10^{-1}$ min	0,35417 $0,24200 \cdot 10^{-1}$ $0,19708 \cdot 10^{-2}$
27,24	$0,2494 \cdot 10^{-2}$ (Γ_γ=0,03)	0,89344 0,640276 0,360078	$0,3494 \cdot 10^{-2}$ max	0,89107 0,68705 0,35444	$0,3494 \cdot 10^{-2}$ max	0,89102 0,68693 0,35431
32,31	$0,9671 \cdot 10^{-1}$	0,876109 0,612515 0,333840	0,10771 max	0,87603 0,61234 0,33366	$0,7571 \cdot 10^{-1}$ min	0,87634 0,61305 0,33439
34,6	$0,42195 \cdot 10^{-1}$	0,973733 0,828261 0,800459	$0,51115 \cdot 10^{-1}$ mid	0,97370 0,89816 0,80028	$0,53195 \cdot 10^{-1}$ max	0,97368 0,89808 0,80017
35,5	$0,2379 \cdot 10^{-2}$	0,908676 0,594741 0,350765	$0,13379 \cdot 10^{-1}$ max	0,90262 0,64299 0,31566	$0,13379 \cdot 10^{-1}$ max	0,90252 0,64268 0,31529
41,42	$0,8006 \cdot 10^{-2}$	0,311426 $0,161792 \cdot 10^{-2}$ $0,42023 \cdot 10^{-4}$	$0,19006 \cdot 10^{-1}$ max	0,24204 $0,16046 \cdot 10^{-2}$ $0,53787 \cdot 10^{-4}$	$0,1 \cdot 10^{-2}$ min	0,33552 $0,16398 \cdot 10^{-2}$ $0,14613 \cdot 10^{-4}$
41,66	$0,38895 \cdot 10^{-1}$	0,550427 $0,410917 \cdot 10^{-1}$ $0,78227 \cdot 10^{-2}$	$0,49895 \cdot 10^{-1}$ max	0,55428 $0,41361 \cdot 10^{-1}$ $0,80729 \cdot 10^{-2}$	$0,49895 \cdot 10^{-1}$ max	0,55418 $0,41305 \cdot 10^{-1}$ $0,80491 \cdot 10^{-2}$
44,48	$0,9964 \cdot 10^{-2}$ (Γ_γ=0,03)	0,328434 $0,313082 \cdot 10^{-1}$ $0,10369 \cdot 10^{-1}$	$0,10964 \cdot 10^{-1}$ max	0,32769 $0,30772 \cdot 10^{-1}$ $0,10105 \cdot 10^{-1}$	$0,12296 \cdot 10^{-6}$ min	0,37812 $0,68455 \cdot 10^{-1}$ $0,29309 \cdot 10^{-1}$
47,6	0,19284	0,805163 0,367239 0,137895	0,20384	0,80484 0,36673 0,13742	0,17184	0,80576 0,36660 0,13917
49,71	0,85692	0,29853 $0,391344 \cdot 10^{-1}$ $0,777378 \cdot 10^{-2}$	0,86792	0,29695 $0,39279 \cdot 10^{-1}$ $0,78167 \cdot 10^{-2}$	0,86792	0,29895 $0,39279 \cdot 10^{-1}$ $0,78167 \cdot 10^{-2}$

UDK 539.173.4

PROMPT NEUTRON SPECTRA FOR THE ENERGY RANGE 10 keV-3 MeV FROM ^{239}Pu AND ^{233}U FISSION BY THERMAL NEUTRONS

A. Lajtai, J. Kechkemeti, J. Shafar, M. Khorany,
D. Kluge, P.P. D'yachenko, V.M. Piksajkin

It is generally known that ^{239}Pu and ^{233}U are considered to be the basic fuel for nuclear power plants utilizing fast reactors. A comprehensive study of the nuclear physics characteristics of these isotopes is accordingly of great interest. The fission neutron spectrum is one of these characteristics and a substantial number of papers has been devoted to it. Most of them, however, deal with the energy region above 1 MeV. The neutron energy range between 0 and 1 MeV, which accounts for some 25% of fission spectrum neutrons, has had only one paper [1] devoted to it. The conclusions of this study, together with the relevant data on ^{235}U [1, 2] and ^{252}Cf [1, 3-7], indicate that the method currently used in reactor calculations to obtain information on the neutron spectrum for this energy range (extrapolation from the higher energy range using the Maxwell or Watt formulae) can at present hardly be considered adequately substantiated.

Our present work was aimed at studying prompt neutron spectra in the 10 keV to 3 MeV range for thermal neutron fission of ^{239}Pu and ^{233}U, using the time-of-flight and the lithium glass method. The measurements were carried out in the tangential channel of the VVRS-M reactor belonging to the Central Institute of Physical Research. The beam was shaped by a special collimator, fast neutrons and γ-quanta being filtered out by means of quartz and polycrystalline bismuth plugs. Figure 1 shows a diagram of the experiment. A scintillation chamber filled with pure argon at atmospheric pressure served as a fission fragment detector. The chamber was so designed that a target prepared from the material being studied and one made of ^{252}Cf having approximately the same characteristics could be introduced alternately into the working volume without adversely affecting the functioning of the apparatus or the geometry of the experiment. In order to optimize the ratio of pulse amplitudes between fission fragments and α-particles (this is particularly important in the case of measurements involving ^{239}Pu), a quartz plate 65 mm in diameter and 0.6 mm thick was positioned at a distance of 9 and 41 mm from the layer of fissile material

and the photomultiplier photocathode respectively. The diameters of all the layers comprised 45 mm. Stainless steel foil 0.1 mm thick served as a support. The layers of ^{239}Pu and ^{233}U were of equal thickness, 1.0 mg/cm^2. The intensity of the fission fragments in the measurements of ^{239}Pu, ^{233}U and ^{252}Cf was 6.4 x 10^3, 5.1 x 10^3 and 2.7 x 10^4 s^{-1} respectively. Number 912 and No. 913 lithium glasses 45 mm in diameter and 9.5 mm thick served as neutron and γ-ray detectors respectively. In order to reduce the background of random coincidences, the neutron and γ-ray detectors were placed within a special shield composed of paraffin, ^6Li hydride and lead. The path length, the analyser channel width and the total prompt γ-ray peak width at half height were 30.5 cm, 0.478 ns and 3 ns respectively. The experimental method is described in Ref. [2].

The measurement procedure for each isotope studied consisted of eight sequentially executed series: ^{239}Pu (^{233}U) - NE-912, ^{239}Pu (^{233}U) - NE-912 (with cone), ^{239}Pu (^{233}U) - NE-913, ^{239}Pu (^{233}U) - NE-913 (with cone) and ^{252}Cf - NE-912, ^{252}Cf - NE-912 (with cone), ^{252}Cf - NE-913, ^{252}Cf - NE-913 (with cone). Aggregate quantities of detected fragments for these series are given in the table. Figure 2 depicts the measured spectra on a time scale. In order to ascertain the correction required for the finite geometry of the experiment, we performed, when measuring the scattered neutron background, an additional experiment using layers of californium 7 and 45 mm in diameter.

In processing the data we applied a relative method which relies on the prompt neutron spectrum from spontaneous fission of ^{252}Cf as a standard. In the first stage all the distributions measured were normalized to a single neutron emitted during fission. Then the background of random and systematic random coincidences was subtracted. Next, the time spectra measured with the NE-913 glass were subtracted from the spectra measured with the NE-912 glass, i.e. the delayed γ-background was taken into account. After this the scattered neutron background was subtracted. Note that, strictly speaking, measurements of the scattered neutron background by the shadow cone method are justified only where a point source is used. Here this was not the case, and accordingly the background measured during the experiment is somewhat understated. The ratio between two time spectra measured in the one case with a small (7 mm diameter) and in the other case a large (45 mm diameter) californium target and the corresponding shadow cones (copper, 12 cm in length) was used to correct for this effect.

It is evident that, given ideal "absolutely black" cones, this ratio will be determined solely by the geometry of the experiment and should not depend on the neutron energy. In our experiment this correction turned out to be 1.20, and it did not change by more than ± 5% in the energy range which was being studied.

Subsequently the distributions obtained were converted to an energy scale, the neutron detection efficiencies were determined (from measured ^{252}Cf spectra, on the assumption that they can be described by a single-parameter distribution with T = 1.42 MeV), and prompt neutron energy spectra for thermal fission of ^{239}Pu and ^{233}U (Figs 3, 4) were ascertained.

The results of extrapolating data from the higher energy region by means of single-parameter Maxwell distributions, with T = 1.38 MeV for ^{239}Pu and 1.32 MeV for ^{233}U, are also shown in these two figures.

It will be seen that, within the experimental error limits (approx. 5%) the neutron spectra of both isotopes in the 10 keV to 3 MeV range are satisfactorily described by these distributions. For ^{239}Pu, this result is consistent with the corresponding data in Ref. [1]. For ^{233}U, however, there is some divergence. In contrast to the present authors' findings, the results of Ref. [1] indicate a ^{233}U fission neutron spectrum 5 to 10% above the Maxwellian distribution in the 0.05–0.3 MeV range.

In conclusion it should be remarked once again that the data in the experiment we have described was treated by a relative method. For this reason the results it yielded for ^{239}Pu and ^{233}U may be interpreted as follows: if the prompt neutron spectrum from ^{252}Cf spontaneous fission in the 10 keV to 3 MeV range is described by a Maxwellian distribution with T = 1.42 MeV, then the neutron spectra for ^{239}Pu and ^{233}U in this energy region exhibit no deviations (beyond ± 5%) from Maxwellian distributions with T = 1.38 and T = 1.32 MeV respectively (cf. the solid curves in Figs 3 and 4 respectively).

REFERENCES

[1] NEFEDOV, V.N., STAROSTOV, B.I., SEMENOV, A.F., In: Nejtronnaya Fizika (Neutron Physics) (Proceedings 4th All-Union Conference on Neutron Physics, Kiev, 18-22 April 1977), Moscow, TsNIIatominform Part 3, (1977), 205; preprint of NIIAR P-22 (356) (1978).

[2] LAJTAI, A., KECHKEMETI, J., KLUGE, D. et al., Ibid, 26.

[3] MEADOWS, J.W., Phys. Rev., 1967, v. 157, p. 1076.

[4] ZAMYATHIN, J.S., KROSHKIN, N.I., MELNIEKOV, A.N., NEFIEDOV, W.N. et al., Nuclear Data for Reactors, Vienna: IAEA, 1970, v. 11, p. 183.

[5] JEKI, L., KLUGE, C., LAJTAI, A. et al., Prompt Fission Neutron Spectra, Vienna: IAEA, 1972, p. 81.

[6] D'YACHENKO, P.P., SEREGINA, E.A., KUTSAEVA, L.S. et al., Atomnaya Ehnergiya 42 (1977) p. 25.

[7] BLINOV, M.V., VITENKO, V.A., TOUSE, V.T., Neutron Standards and Application, NBS Special publ. 493, Washington, 1977, p. 194.

The article was submitted for publication on 5 April 1983.

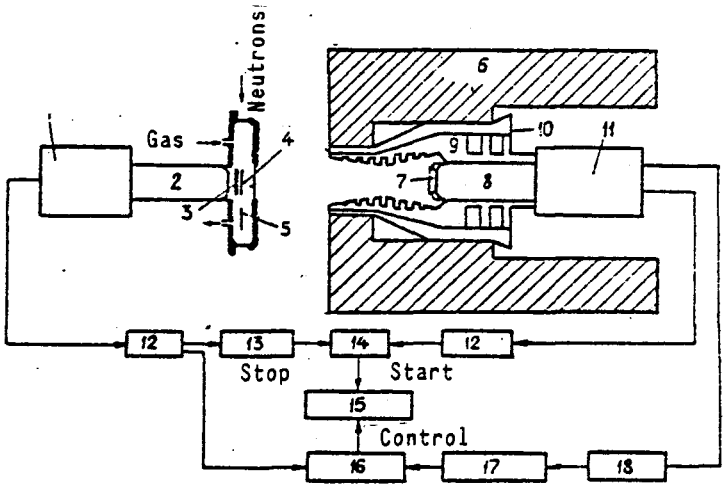

Fig. 1.: Diagram of the experiment

(1) Fission fragment detector
(2) Photomultiplier 56-UVP
(3) Quartz
(4) ^{235}U target
(5) ^{252}Cf target
(6) Paraffin
(7) Lithium glass
(8) Photomultiplier 56-UVP
(9) Lead
(10) ^{6}Li hydride
(11) Neutron (γ-ray detector)
(12) Discriminator with follow threshold
(13) Delay line
(14) Time-amplitude converter
(15) Analyser
(16) Coincidence circuit
(17) Differential discriminator
(18) Amplifier

Numbers of fragments recorded (x 10^9)

Neutron (γ-ray) detectors	^{239}Pu	^{233}U	^{252}Cf
NE-912	7,789	10,800	11,065
NE-913	7,734	12,713	12,254
NE-912 (with cone)	9,114	8,600	19,212
NE-913 (with cone)	5,95	12,229	37,090

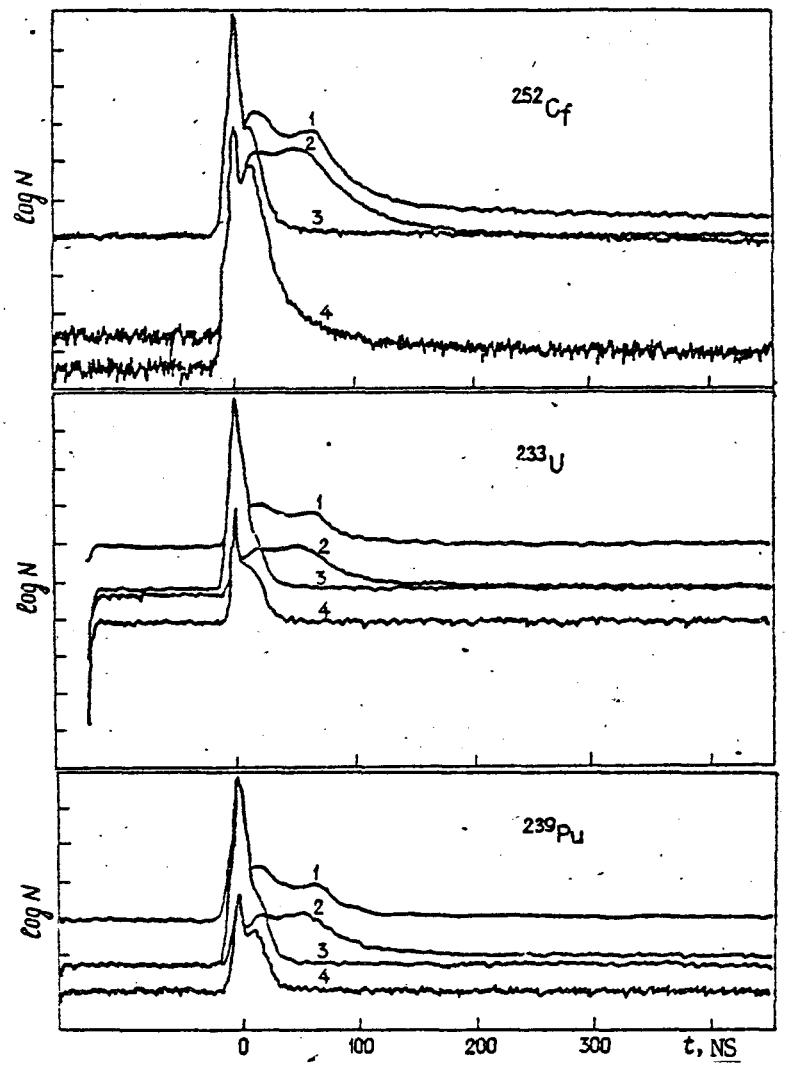

Fig. 2.: Measured spectra on a time scale:
1 - NE-912; 2 - NE-913; 3 - NE-912 (copper);
4 - NE-913 (copper)

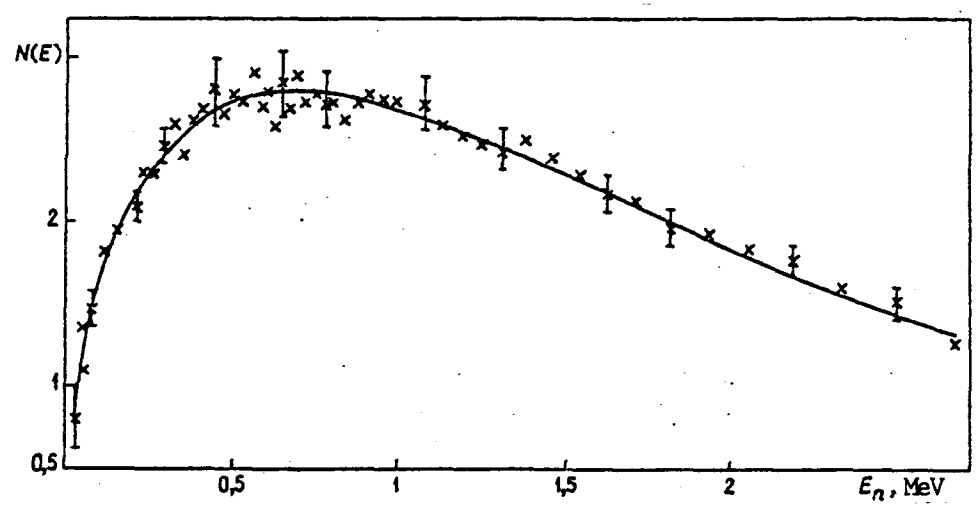

Fig. 3.: Prompt neutron spectrum from thermal fission of ^{239}Pu.

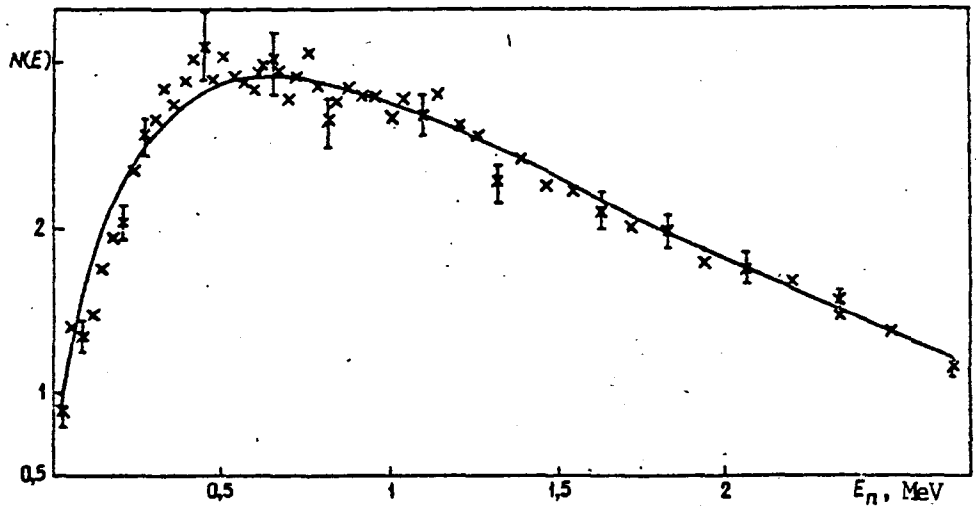

Fig. 4.: Prompt neutron spectrum from thermal fission of ^{233}U.

UDK 539.173.84+543.53

OPTIMIZATION OF DELAYED NEUTRON DETECTION UNITS FOR ACTIVATION ANALYSIS OF URANIUM AND THORIUM

E.G. Bertman

Activation analysis of geological materials for uranium and thorium by the delayed neutron method makes special demands on delayed neutron detection units. Increasing the sensitivity of the method requires maximum neutron detection efficiency and minimum background. The six basic groups of delayed neutrons have a half-life of 0.2-1 min. They are therefore detected shortly after irradiation of the sample in the reactor, usually in 10-20 s. In this situation the residual induced γ-activity in the matrix of the geological sample (1-20 g per sample) can be very significant and attain 1000 R/h, a feature which must be allowed for in selecting the neutron detector.

Fission chambers detect neutrons with high selectivity against a background of γ-ray fluxes of virtually any intensity, but have low sensitivity to neutrons. Fast delayed neutrons with a mean energy of 0.49 MeV can easily be moderated by placing the irradiated sample in a moderating medium such as paraffin or water. Slow neutrons, on the other hand, can be detected with extreme sensitivity and efficiency by gas discharge counters with a boron-coated cathode or filled with ^{3}He [1]. Among the gas discharge counters having a high permissible γ-background value (up to 1000 R/h), the SNM-11 corona counter with its 15.5% neutron detection efficiency has the best parameters.

When analysed for thorium, the sample is irradiated by a flux of fast neutrons only, which yields induced γ-activity two orders of magnitude lower than in the analysis for uranium when the sample is irradiated with thermal neutrons. In this case helium counters with a maximum permissible γ-background of 100 and 20 R/h should be used, i.e. types SNM-17 and SNM-18 respectively, the detection efficiency of which attains 80%. The delayed neutron detection unit appears as a cylinder of the moderating medium in the centre of which the sample is positioned after being transported out of the reactor by a pneumatic conveyor. Gas discharge counters are positioned round the channel and sample in a circle of radius R. The optimum number of counters and their distance from the sample can be determined simply and

accurately by experiment in such a way that the counting efficiency of the unit is maximized. The radial distribution of the neutrons from the (Po-α-Be) source in water, paraffin and graphite was measured for different numbers of counters from 1 to 50. One of these counters was used to detect the neutrons, and from this it was possible to determine the optimum radius (7 cm) of the circle on which the counters were placed around the source. The dimensions of the detection unit are determined by the length of the counter and the distribution of neutrons in the moderator. For detection units using water, paraffin or polyethylene as moderator and utilizing counters of types SNM-11, SNM-17 and SNM-18, the optimum height and diameter are 40-50 cm.

The neutron detection efficiency increases with the number of counters used, the number being restricted in the case of short radii by the size of the counters themselves. Positioning the counters close to one another in rows results in displacement of the moderator, and creates a neutron flux depression which reduces the counting efficiency. The authors of Ref. [2] recommend an optimum detection unit with ten counters positioned in a circle with a diameter of 20 cm. From our own experiments we conclude that for moderators containing hydrogen the optimum number of counters is 20. Further increasing their number does not achieve any material increase in the neutron count rate N and merely complicates and raises the cost of the detection unit and its electronic circuitry. In Table 1 we compare detection efficiencies ε for units with different moderators and 20 counters of types SNM-11 and SNM-18. It is evident that a unit using water as moderator and counters of type SNM-18 has the highest efficiency - 33%.

Another means of increasing the sensitivity of the delayed neutron method is to use a subcritical breeder assembly to amplify the low neutron fluxes emitted by the sample. The experiments were carried out for a breeder with a heterogeneous core whose dimensions, like the mass of the fissile material, were well below critical. The multiplication constant was considerably less than unity, which simplified the design and control of the assembly. The measurements were carried out in a geometry with 20 type SNM-11 counters installed in the water moderator around a circle with a radius of 7 cm. A ^{252}Cf neutron source was placed in the centre, the source being surrounded (R = 4.4 cm) by a cylindrical multiplier of variable thickness consisting of uranium enriched to 95% in ^{235}U.

The multiplication constants of the detected neutrons as a function of ^{235}U thickness are shown below:

Thickness, mm:	0	0.4	0.8	1.2	1.6
C_m:	1.0	1.48	1.50	1.58	1.68

It follows from these data that the multiplication constant for the neutrons detected, C_m, which is equal to the ratio between the count rate with a multiplying medium and the count rate without, rises to 1.48 even for a ^{235}U thickness of 0.4 mm. Increasing the thickness of the multiplier further has much less effect: at a thickness of 1.6 mm we find $C_m = 1.68$.

The detection efficiency can be raised by 68% if we use a delayed neutron detection unit with a heterogeneous multiplier. A multiplier with a homogeneous zone enables the efficiency to be increased by 2-3 orders of magnitude, as rough calculations have shown. It must, however, be borne in mind that using a multiplier in the detection unit increases the numbers of useful and of background neutrons in equal measure. Since the neutron multiplication effect results from fissions in the multiplier substance, the emission of delayed neutrons is also a consequence of this process. The latter have a half-life comparable to the detection time in analysing samples for uranium and thorium. This can lead to an accumulation factor which influences the count rate when only brief intervals occur between two or three consecutive analyses.

Table 2 gives measurements of the delayed neutron background from a multiplier consisting of 95% enriched ^{235}U (a cylinder with h = 50 cm, R = 4.4 cm, d = 2.4 mm) after irradiation with neutrons from a ^{252}Cf source ($\Phi = 1.45 \times 10^{7}$ n · s^{-1}) for 60 seconds without additional shielding against external background neutrons. These results support the assumptions expressed above. However, the ratio of background delayed neutrons to the number of neutrons detected from the source is rather low (8×10^{-4}). Since in analyses of natural objects the intensity of the delayed neutrons emitted by the sample is much lower than in the case of the ^{252}Cf source used in the experiments, the contribution of background delayed neutrons will be so small that it may be ignored altogether.

Experiments with delayed neutrons have indicated a detection efficiency 5.5 times greater than for neutrons from ^{252}Cf or Pu-α-Be sources. The results for units with a paraffin moderator and 20 counters of types SNM-11, SNM-17 and SNM-18 are given in Table 3.

A full-scale set-up for analysing geological samples by the delayed neutron method should be equipped with two detection units: type SNM-11 without a multiplier for uranium analysis and SNM-18 with a multiplier for thorium analysis.

REFERENCES

[1] KOROLEV, V.I., CHAJKOVSKIJ, V.G., Pribory i tekhnika ehksperimenta (Experimental instruments and techniques) No. 4 (1969) 208.

[2] VOROB'EV, Yu.A., UGOL'TSEV, O.A., In: Transactions of the Second All-Union Conference on the Metrology of Neutron Radiation in Reactors and Accelerators, Vol. 1, Moscow (1974) 90.

The article was submitted for publication on 7 February 1983.

Table 1. Detection efficiency for a neutron flux with 4.8×10^3 $n \cdot s^{-1}$ from a (Pu-α-Be) source, obtained with a unit using 20 SNM-11 and SNM-18 counters in various moderators

Moderator dimensions	Optimiz. radius, cm	SNM-11		SNM-18	
		N, c/s	ε, %	N, c/s	ε, %
Water, 50 x 50 cm	7	230	4.8	1580	33
Paraffin, 50 x 50 x 50 cm	7	220	4.6	1440	30
Paraffin with bismuth shield, 60 x 60 x 60 cm	11	153	3.2	1150	24
Polyethylene, 40 x 40 x 40 cm	7.5	216	4.5	1390	29
Graphite, 40 x 40 x 40 cm	12	48	0.1	62	1.3

Table 2. Dependence of multiplier delayer neutron background on measurement time

Background, c/s	Seconds after irradiation					
	10	20	30	40	50	60
With multiplier	78	30	16	10	8	6
Without multiplier	7	8	6	8	7	6

Table 3. Parameters of neutron detection units

Parameters	SNM-11	SNM-17	SNM-18
Delayed neutron detection efficiency, %:			
Without multiplier	25	64	78
With multiplier	42	108	131
Permissible background of γ-radiation	1000	100	20

UDK 539.172.12

SYSTEMATICS OF NUCLEAR REACTION YIELDS FOR A THICK TARGET BOMBARDED WITH 22 MeV PROTONS

P.P. Dmitriev

Reference [1] presents 188 experimental yields for 140 radioactive nuclides, obtained by irradiating thick targets of various chemical elements with 22 MeV protons. The reactions which produced the nuclides are also given: pn, p2n, ppn, p(pn+2n), p2p, p3n, pα, pαn, and so on. The large volume of data on nuclide yields presented in Ref. [1] allows us to compare yields from reactions of various types with yields from reactions of a single type for a broad range of nuclear masses.

The yield of a reaction can be defined as the quantity of reaction events per 1000 bombarding particles. For each event of a given reaction, an atom of a certain radionuclide is formed. If irradiating a chemical element produces a radionuclide through only one reaction, the reaction yield can be ascertained from the radionuclide yield by the following formula:

$$W = 0.554 Z_a T_{1/2} (B/P_c), \qquad (1)$$

where W is the reaction yield in atoms per 1000 particles; Z_a is the relative charge of the bombarding particle; $T_{1/2}$ is the nuclide's half-life in days; B is the radionuclide yield in MBq/(μA·h); P_c is the content of target isotope, in %. The following formula links the reaction yield with the effective reaction cross-section averaged over the mean free path of the incident particle:

$$\bar{\sigma} = 1.66\ 10^3 W(A/R), \qquad (2)$$

where $\bar{\sigma}$ is the effective cross-section, in mb; A is the relative atomic mass of the element; and R is the mean free path of the particle, in mg/cm^2. From formula (1), using the quantity P_c, we can determine both the reaction yield and the reaction cross-section for a target isotope concentration of 100%.

In this paper most of the radionuclide yields presented in Ref. [1] have been converted to yield values for nuclear reactions of a particular kind and have been classified according to the type of reaction. After Ref. [1] had been submitted for printing the yields of eight radionuclides were measured: ^{45}Ti(Sc), ^{87m}Y(Sr), ^{87}Y(Zr), ^{89}Zr(Zr); ^{91m}Nb(Zr), ^{117}Sn(Sn),

^{117}Sb(Sn), ^{193}Au(Pt) for E_p = 22 MeV (the irradiated elements are shown in brackets). These yields have also been converted to reaction yields. The results of the calculations are given in the table. Yields were determined for 185 reactions in all (the number of reactions is given in brackets) of the following types: pn (59), p2n (44), ppn (23), p(pn+2n) (13), p3n (13), pα (7), p2p (6), pαn (6), p(pn+2p) (5), pαn (6), pt (5), p(t+3n) (2), pαp (1), pα2n (1).

As can be seen from Ref. [1] (Table 1, column 3), radionuclides result from one or several reactions. If a radionuclide results from a single reaction, the reaction yield is determined by formula (1). For example, if copper is irradiated the ^{65}Zn yield is 0.59 MBq/(μA·h), the reaction of interest is ^{65}Cu(pn)^{65}Zn, P_c = 30.9%, and the reaction yield given by Eq. (1) is W = 2.6 atoms/1000 protons. Reactions resulting in a cumulative yield have the same nucleus target, and the reaction yield is calculated from Eq. (1). For example, if germanium is irradiated the cumulative yield of ^{69}Ge from the ^{70}Ge(ppn)^{69}Ge and ^{70}Ge(p2n)^{69}As ($T_{1/2}$ = 15.2 min) ^{69}Ge reactions is 61 MBq(μA·h), P_c = 20.6%, and the reaction yield of ^{70}Ge(p, pn+2n)^{69}Ge is W = 2.7 atoms/1000 protons.

Very frequently a radionuclide can be formed through several reactions for which various stable isotopes of the irradiated element serve as target nuclei. In many cases it is possible both to identify the reaction which makes the largest contribution to the nuclide yield and to determine the yield of this reaction. The yield of the main reaction can be calculated by the formula

$$W_o = (W_n 100 - W_1 P_1 - W_2 P_2 - \ldots)/P_o, \qquad (3)$$

where W_n is the total yield of all reactions (atoms/1000 protons) calculated from the measured yield of the radionuclide by means of formula (1) for P_c = 100%; W_1, W_2... are the yields of other reactions making a lesser contribution to the radionuclide's yield, in atoms/1000 protons; P_1, P_2... is the concentration of target isotopes for other reactions, in %; and P_o is the target isotope concentration for the main reaction, in %.

Experimental values of W_1, W_2... are unknown, so in their place we use average values of known yields for reactions of this type in the appropriate nuclear mass range. Let us consider a practical example of how to calculate the yield of the main reaction from Eq. (3). In Ref. [1] we show (Table 1) that irradiation of neodymium produces ^{143}Pm through pn, p2n, p3n reactions: ^{143}Nd (12.2%) (pn), ^{144}Nd (23.87%) (p2n), ^{145}Nd (8.3%) (p3n) (the concentrations of ^{143}, ^{144}, ^{145}Nd in natural neodymium are given in brackets); the ^{143}Pm yield is 0.59 MBq(μA·h). The table below shows that in the given nuclear mass region the p2n reaction has a substantially higher yield than the pn and p3n reactions and that the ^{144}Nd concentration is higher than that of ^{143}Nd and ^{145}Nd. This is why the ^{144}Nd (p2n)^{143}Pm reaction makes the largest contribution to the ^{143}Pm yield and constitutes the main reaction. From the table we find that W_1 = 0.19 atoms/1000 protons from the ^{143}Nd (pn)^{143}Pm reaction constitutes the mean of the pn reaction yields for the ^{139}La, ^{154}Sm and ^{153}Eu nuclei. Similarly, values of the p3m reaction yields for ^{128}Tl, ^{152}Sm and ^{170}Er give W_2 = 0.32 atoms/protons for the ^{145}Nd (p3n)^{143}Pm reaction. The total yield from all reactions leading to the formation of ^{143}Pm is $W_n = 0.554\ T_{1/2}\ (B/100) = 0.86$ atoms/1000 protons. Now all the quantities needed to compute the yield of the ^{144}Nd (p2n)^{143}Pm reaction using formula (3) have been defined: W_o = 3.4 atoms/1000 protons.

The main reaction yield calculated from Eq. (3) contains an error due to the uncertainty in the values of W_1, W_2... used. Where, however, the contribution of other reactions to the nuclide yield is small, the errors in W_1, W_2... do not significantly affect W_o. For the purposes of the present example, if we use values of W_1 and W_2 which are increased or reduced by a factor of 1.5, the yield W_o will differ by only 0.1 from the quantity 3.4 while changing the values of W_1 and W_2 by a factor of 2 will change W_o by 0.2.

Let us now evaluate the contribution of the pn and p3n reactions to the yield of ^{143}Pm for W_1 = 0.19 atoms/1000 protons and W_2 = 0.32 atoms/1000 protons. From Eq. (1) we obtain:

$$B = 1.81WP_c/(Z_aT_{1/2}). \qquad (4)$$

The yield of ^{143}Pm given by Eq. (4) for the ^{143}Nd(pn)^{143}Pm reaction is B_1 = 0.016 MBq/(μA·h), and for the ^{145}Nd(p3n)^{143}Pm reaction B_2 = 0.018 MBq/(μA·h); the combined yield is 0.034 MBq/(μA·h), which accounts for 5.8% of the total ^{143}Pm yield [0.59 MBq/(μA·h)]. Consequently, when the contribution

of other reactions to the nuclide yield is approximately 6%, a change in W_1, W_2 by a factor of 1.5 or even 2 does not materially alter the main reaction yield. Obviously, when the contribution of other reactions to the radionuclide yield is greater, changes in W_1, W_2 will influence the size of the yield from the main reaction more powerfully. The following example illustrates this. Irradiating platinum produces ^{194}Au through the reactions ^{194}Pt(pn), ^{195}Pt(p2n) and ^{196}Pt(p3n), and the ^{194}Au yield is 78 MBq/(μA·h) (see Ref. [1], Table 1). From the table in this paper it can be seen that in this nuclear mass range the p2n reaction yield is markedly higher than the pn and p3n reaction yields. Let us calculate the yield of the ^{195}Pt(p2n)^{194}Pt reactions from Eq. (3), using the data in our present table to find W_1 and W_2. We define the yield of the ^{194}Pt(pn)^{194}Au reaction as the mean yield of the pn reactions on ^{184}W, ^{197}Au and ^{202}Hg: W_1 = 0.13 atoms/1000 protons; the yield of the ^{196}Pt(p3n)^{194}Au reaction as the mean yield of the p3n reaction on ^{187}Re, ^{202}Hg, ^{204}Hg and ^{203}Tl: W_2 = 0.47 atoms/1000 protons. Given these values of W_1 and W_2, the yield of the ^{195}Pt(p2n)^{194}Au reaction amounts to W_o = 1.6 atoms/1000 protons. If we increase W_1 and W_2 by a factor of 1.5, we reduce W_o by 13%; and if we reduce W_1 and W_2 by a factor of 1.5, W_o is increased by 8%. The combined contribution of pn and p3n reactions to the ^{194}Au yield, given these values of W_1 and W_2, is 23% of the ^{194}Au yield. Calculating the reaction yield from Eq. (3), we first determined the contribution of other reactions to the radionuclide yield for the given values of W_1, W_2; the main reaction yield was calculated in those cases where the contribution of other reactions to the radionuclide yield did not exceed approximately 25%. We may assume that with this procedure the error is W_o due to the uncertainty in the W_1, W_2... values used does not exceed 10–15%; this is approximately equal to the error in the experimental radionuclide yields quoted in Ref. [1]. Cases where the reaction yield was calculated from Eq. (3) are identified in the table by the letters "mr" (main reaction). In the overwhelming majority of our calculations the contribution of other reactions was less than 10%. The yields obtained from Eq. (3) were a valuable supplement to the reaction yield data.

Let us consider one other method of determining reaction yields. If a nuclide is formed from two reactions whose thresholds differ markedly from one another, the yield of each reaction can in some cases be ascertained from the curve of the nuclide yield versus proton energy. Typical examples are the experimental curves of the ^{113}Sn [2] and ^{203}Pb [3] yields resulting from the irradiation of indium and thallium. In both cases the nuclide is formed by the pn and p3n reactions. Up to the threshold of the p3n reaction at approximately 18 MeV the nuclide is formed only via the pn reaction; when the proton energy exceeds 18 MeV we can observe a rapid increase in the nuclide yield as the p3n reaction comes into play. Extrapolating the nuclide yield curve due to the pn reaction from E_p = 18 MeV to E_p = 22 MeV, we can obtain the nuclide yield at E_p = 22 MeV due to the pn reaction alone. The difference between the total nuclide yield and the yield from the pn reaction gives the nuclide yield from the p3n reaction at E_p = 22 MeV. From the nuclide yields found in the pn and p3n reactions we can calculate the pn and p3n reaction yields using Eq. (1). The reaction yields determined in this way are identified in the table by the letters "yc" (yield curve). The ^{110}In^m and ^{111}In yield in the pn and p2n reactions was measured by irradiating enriched ^{111}Cd and ^{112}Cd (98% enrichment). The yields of these reactions are identified by "enr".

Certain patterns can be observed in the way reaction yields change as the atomic number of the target nucleus increases: the pn reaction yield diminishes while that of the p3n reactions increases. In the case of p2n and ppn reactions, the yield has a certain maximum value, and the ppn reaction yield changes relatively little. Careful study of the table will reveal other patterns which can be explained if we take into account the change in nuclear binding energy per nucleon, the magnitude of the reaction thresholds, the role of the Coulomb barrier and the specific reaction mechanism. It is also clear that the yield of isomer formation reactions is substantially lower, a fact which is evidently accounted for by the lower probability of levels with higher spin being populated in the final excited nucleus. The anomalously high yield of the ^{58}Ni(p2p)^{57}Co reaction is of special interest here.

The reaction yield values shown in the table are of practical use in evaluating the yields of various radionuclides obtained when targets are irradiated with 22 MeV protons and protons at other energy levels. To estimate the radionuclide yield obtained with protons of different energies, we can make use of the relative behaviour of the nuclide yield curves for reactions of a particular type - pn, p2n, ppn and so on - in the nuclear mass range of interest. Normalizing the relative shape of the nuclide yield curve to a value of W (for E_p = 22 MeV) selected on the basis of the data in the table, we obtain from the normalized curve values of W for the selected reaction type at E_p = 22 MeV. The radionuclide yield for the value obtained is then calculated by means of Eq. (4). Examples of radionuclide yield curves for various types of reactions with protons can be found in Ref. [4].

It is proposed to publish systematized data on nuclear reaction yields for 22 MeV deuterons and 44 MeV α-particles.

The paper was submitted for publication on 21 March 1983.

REFERENCES

[1] DMITRIEV, P.P., MOLIN, G.A., Voprosy atomnoj nauki i tekhniki (Problems of atomic science and technology), Nuclear constants series, No. 5(44) (1981) 43.

[2] DMITRIEV, P.P. et al., Atomnaya Ehnergiya, 39 (1975) 135.

[3] DMITRIEV, P.P. et al., Ibid, 38 (1974) 100.

[4] DMITRIEV, P.P. et al., Ibid, 20 (1966) 154; 21 (1966) 52; 22 (1967) 310; 23 (1967) 61; 23 (1968) 278-279; 26 (1969) 467; 27 (1969) 13,125,208; 28 (1970) 503; 29 (1970) 205-206; 32 (1972) 774; 34 (1973) 404-405; 35 (1973) 61; 41 (1976) 38,431; 42 (1977) 148; 46 (1979) 53; 48 (1980) 122,402; 49 (1982) 329; 52 (1982) 72; 53 (1982) 198.

Table

Yields from reactions of various types for a thick target bombarded by 22 MeV protons

Target nucleus	Product nucleus	Reaction yield, atoms/1000 protons	Target nucleus	Product nucleus	Reaction yield, atoms/1000 protons	Target nucleus	Product nucleus	Reaction yield, atoms/1000 protons
	pn		^{66}Zn	^{66}Ga	0,56 br	^{110}Cd	^{110m}In	0,33 enr*
^{7}Li	^{7}Be	3,4	^{69}Ga	^{69}Ge	I,4	^{111}In	^{111}In	0,93 enr
^{11}B	^{11}C	2,6	^{72}Ge	^{72}As	2,4 br	^{114}Cd	^{114m}In	0,38 br
^{13}C	^{13}N	I,7	^{74}Ge	^{74}As	I,9	^{113}In	^{113}Sn	I,I yc*
^{18}O	^{18}F	3,2	^{76}Ge	^{76}As	0,76	^{120}Sn	^{120m}Sb	0,I2 br
^{26}Mg	^{26}Al	0,64	^{75}As	^{75}Se	I,3	^{122}Sn	^{122}Sb	I,0 br
^{44}Ca	^{44m}Sc	0,4I	^{82}Se	^{82}Br	0,95	^{124}Sn	^{124}Sb	0,52
^{44}Ca	^{44g}Sc	I,3	^{79}Br	^{79}Kr	I,I	^{121}Sb	^{121m}Te	0,3I br
^{45}Sc	^{45}Ti	0,62	^{85}Rb	^{85}Sr	I,3	^{121}Sb	^{121g}Te	0,47 br
^{48}Ti	^{48}V	2,6 br*	^{88}Sr	^{88}Y	2,4	^{123}Sb	^{123m}Te	0,24
^{51}V	^{51}Cr	3,I	^{89}Y	^{89}Zr	0,70	^{126}Te	^{126}I	I,I br
^{52}Cr	^{52}Mn	0,7I br	^{92}Zr	^{92m}Nb	0,78 br	^{130}Te	^{130}I	0,32
^{54}Cr	^{54}Mn	I,2	^{93}Nb	^{93m}Mo	0,048	^{127}I	^{127}Xe	0,33
^{55}Mn	^{55}Fe	I,5	^{93}Nb	^{93}Mo	0,088	^{133}Cs	^{133m}Ba	0,I7
^{56}Fe	^{56}Co	I,3 br	^{103}Rh	^{103}Pd	I,I	^{133}Cs	^{133}Ba	0,46
^{57}Fe	^{57}Co	I,2 br	^{107}Ag	^{107}Cd	I,0 br	^{139}La	^{139}Ce	0,34
^{65}Cu	^{65}Zn	2,6	^{109}Ag	^{109}Cd	I,0	^{154}Sm	^{154}Eu	0,I3

* The meaning of "br", "yc" and "enr" is explained in the text.

Target nucleus	Product nucleus	Reaction yield, atoms/1000 protons
^{153}Eu	^{153}Gd	0,II
^{168}Er	^{168}Tm	0,I8 br
^{170}Er	^{170}Tm	0,08
^{181}Ta	^{181}W	0,082
^{184}W	^{184m}Re	0,0066 yc
^{184}W	^{184g}Re	0,I3 yc
^{197}Au	^{197}Hg	0,I4
^{202}Hg	^{202}Tl	0,099 yc
^{203}Tl	^{203}Pb	0,I3 yc
p2n		
^{48}Ca	^{47}Sc	0,47
^{45}Sc	^{44}Ti	0,I4
^{56}Fe	^{55}Co	0,II
^{63}Cu	^{62}Zn	0,32
^{68}Zn	^{67}Ga	2,6 br
^{69}Ga	^{68}Ge	I,8
^{72}Ge	^{71}As	I,7
^{74}Ge	^{73}As	2,I br
^{88}Sr	^{87m}Y	0,072 br
^{88}Sr	^{87}Y	I,8 br
^{89}Y	^{88}Zr	0,89
^{92}Zr	^{91m}Nb	0,I6
^{96}Zr	^{95}Nb	I,7
^{98}Mo	^{97m}Tc	0,70 br
^{102}Ru	^{101m}Rh	I,9 br
^{111}Cd	^{110m}In	0,65 enr
^{112}Cd	^{111}In	2,0 enr
^{118}Sn	^{117}Sb	3,4 br
^{124}Te	^{123}I	2,6 br
^{125}Te	^{124}I	2,8 br
^{126}Te	^{125}I	I,9 br
^{136}Ba	^{135}La	0,80 br
^{140}Ce	^{139}Pr	I,I
^{141}Pr	^{140}Nd	I,7
^{144}Nd	^{143}Pm	3,4
^{148}Sm	^{147}Eu	2,2 br
^{149}Sm	^{148}Eu	I,0 br
^{166}Er	^{165}Tm	I,2 br
^{168}Er	^{167}Tm	I,7 br
^{174}Yb	^{173}Lu	2,5 br
^{177}Hf	^{176}Ta	0,7 br
^{178}Hf	^{177}Ta	I,5 br
^{182}W	^{181}Re	I,6 br
^{183}W	^{182m}Re	0,52 yc
^{183}W	^{182g}Re	0,62 yc
^{184}W	^{183}Re	I,5 br
^{194}Pt	^{193}Au	I,5 br
^{195}Pt	^{194}Au	I,6 br
^{196}Pt	^{195}Au	0,47 br
^{201}Hg	^{200}Tl	0,8I br
^{202}Hg	^{201}Tl	I,7 br
^{203}Tl	^{202m}Pb	0,I8
^{206}Pb	^{205}Bi	2,I br
^{208}Pb	^{207}Bi	I,7
ppn		
^{14}N	^{13}N	0,67 br
^{27}Al	^{26}Al	0,53
^{45}Sc	^{44m}Sc	0,48
^{55}Mn	^{54}Mn	I,4
^{59}Co	^{58}Co	I,6
^{65}Cu	^{64}Cu	I,2
^{75}As	^{74}As	0,35
^{85}Rb	^{84}Rb	0,I3
^{89}Y	^{88}Y	0,25
^{93}Nb	^{92m}Nb	0,I2
^{103}Rh	^{102m}Rh	0,I4
^{103}Rh	^{102g}Rh	0,3I
^{107}Ag	^{106m}Ag	0,094
^{109}Ag	^{108m}Ag	0,0072
^{115}In	^{114m}In	0,I2
^{118}Sn	^{117m}Sn	0,064 br
^{127}I	^{126}I	0,I3
^{133}Cs	^{132}Cs	0,062
^{130}Ba	^{135m}Ba	0,068
^{151}Eu	^{150m}Eu	0,I6
^{153}Eu	^{152}Eu	0,22
^{197}Au	^{196}Au	0,062
^{203}Tl	^{202}Tl	0,022
p(pn+2n)		
^{19}F	^{18}F	I,4
^{23}Na	^{22}Na	I,2
^{52}Cr	^{51}Cr	I,I br
^{56}Fe	^{55}Fe	I,6 br
^{58}Ni	^{57}Ni	0,39
^{66}Zn	^{65}Zn	I,9 br
^{70}Ge	^{69}Ge	2,7
^{76}Se	^{75}Se	I,7 br
^{86}Sr	^{85}Sr	0,76 br
^{90}Zr	^{89}Zr	I,I br
^{110}Cd	^{109}Cd	I,6 br
^{114}Sn	^{113}Sn	I,I br
^{140}Ce	^{139}Ce	I,I
p3n		
^{115}In	^{113}Sn	0,044 yc
^{128}Te	^{126}I	0,I8 yc
^{152}Sm	^{150m}Eu	0,25 br
^{170}Er	^{168}Tm	0,52 yc
^{184}W	^{182m}Re	0,I6 yc
^{184}W	^{182g}Re	0,3I yc
^{186}W	^{184m}Re	0,088 yc
^{186}W	^{184g}Re	0,78 yc
^{187}Re	^{185}Os	0,93 br
^{202}Hg	^{200}Tl	0,52 yc
^{204}Hg	^{202}Tl	0,34 yc
^{203}Tl	^{201}Pb	0,2I
^{205}Tl	^{203}Pb	0,50 yc
pα		
^{14}N	^{11}C	I,6 br
^{16}O	^{13}N	0,37 br
^{25}Mg	^{22}Na	0,85 br
^{49}Ti	^{46}Sc	0,3I br
^{58}Ni	^{55}Co	0,I0 br
^{70}Ge	^{67}Ga	0,20 br
^{90}Zr	^{87}Y	0,036
p2p		
^{25}Mg	^{24}Na	0,I3 br
^{43}Ca	^{42}K	0,0I7 br
^{44}Ca	^{43}K	0,0043 br
^{58}Ni	^{57}Co	2,4 br
^{61}Ni	^{60}Co	0,II br
^{68}Zn	^{67}Cu	0,0034
p(pn+2p)		
^{12}C	^{11}C	0,28
^{48}Ca	^{47}Ca	0,I0
^{96}Zr	^{95}Zr	0,38
^{116}Cd	^{115}Cd	0,I2
^{204}Hg	^{203}Hg	0,064
pαn		
^{55}Mn	^{51}Cr	0,09I
^{62}Ni	^{58}Co	0,33 br
^{69}Ga	^{65}Zn	0,2
^{88}Sr	^{84}Rb	0,I0 br
^{93}Nb	^{89}Zr	0,037
^{139}La	^{135m}Ba	0,057 br
pt		
^{9}Be	^{7}Be	0,I4
^{51}V	^{49}V	0,0068 br
^{58}Ni	^{56}Ni	0,0II
^{59}Co	^{57}Co	0,0I4
^{79}Br	^{77}Br	0,II
p(t+3n)		
^{103}Rh	^{101m}Rh	0,0I7
^{209}Bi	^{207}Bi	0,2I
pαp		
^{51}V	^{47}Sc	0,037
pα2n		
^{110}Cd	^{105}Ag	0,I3 br

UDK 539.1.07

AN INTEGRATED HARDWARE/SOFTWARE CONFIGURATION FOR THE EVALUATION OF NUCLEAR DATA

A.G. Zvenigorodskij, V.A. Agureev, I.B. Dunaev, S.A. Dunaeva,
G.A. Lomtev., V.N. Matvej, A.F. Shapovalov

The large volume of data which an evaluator has to process in order to obtain recommended constants is the determining factor in evaluation work. Reference [1] describes a data bank set up to make the evaluator's work more efficient. Today, the use of a data bank without man-machine interaction by means of computer graphics would be unthinkable. Man-machine interaction in this context means not only the hardware and software required for data storage and retrieval in a nuclear data bank but also a simple and reliable means of entering the data into the bank from a range of data carriers. Experience shows that organizing the collection of data presented in graphic and tabular form is a vital aspect of this task.

In order to carry out his evaluation, the physicist must have the following technical resources at his disposal: (1) digitized versions of the graphics with subsequent recording of the digitized data onto a machine carrier or direct to the computer; (2) visualization of the input on a display unit; (3) direct access to a central data bank from remote terminals; and (4) buffered input and review of all data entered. The software must include input and edit programs for all data and ancillary information entered and also format modification programs. The article reviews a hardware/software configuration designed along modular lines for tasks involving graphically presented information.

Hardware

The basic set of hardware modules required to process graphical data includes (Fig. 1):

- An acoustic device for digitizing graphics, a so-called acoustic pen (AP);
- A device to display graphics data on the CRT screen (GDD);
- Magnetic tape storage;

- An alpha-numeric display unit with an attachment for graphics generation;
- A wide-range, high-speed recorder;
- A type "Ehlektronika DZ-28" microcomputer; and
- A PL-150 perforator.

All these modules are combined in an integrated system by means of a shared data line (SDL) of type MEhK 625.1 [2]. The SDL MEhK 625.1 system was chosen as the main line, firstly because it is relatively simple, secondly because it can be used as the basis for simple, controllerless systems of the "transmitter only-receiver only" type, and thirdly because this standard is coming into ever wider use at the present time.

Graphics digitizer. Acoustic pen (AP)

The acoustic digitizer for graphical information consists of a plotting screen on which graphics can be set out or projected; a spark pen which generates a sound-wave at the point of contact; and a control unit and an interface unit. When the spark discharger at the tip of the pen is activated, the counters begin to record X and Y impulses generated by the master clock. The clock ceases to function when the sound-wave reaches the linear microphones mounted round the edges of the plotting screen. In order to prevent low-frequency sound from being superimposed on the desired signal, electrical oscillations from the microphones are fed to amplifiers with a restricted transmission band.

After the fast discriminators have been tripped by the steep leading edge of the oscillations (this also stops the master clock), numbers proportional to the distances from the discharger to the microphones are formed in the X and Y counters. The co-ordinate pair thus obtained is transformed into a sequence of octal coded messages in the KOI-7 codes and is then transmitted to the SDL by means of 8 bytes. The codes for the symbols "line feed" and "carriage return" are transmitted at the end of the message. In addition, command data such as "write to internal memory", "delete period", "tape marker write-in" etc. can be transmitted via the SDL to the receiving terminal. There are control buttons for this purpose located on the front panel of the acoustic pen control unit. The plotter has a working area of 350 mm^2, the

number of dots is 1024 x 1024, and instrument error is $\pm$ 0.35 mm. The AP interface is fully consistent with the standard [2] and can carry out an interrupt function in addition to the data transmission function.

Device for graphics display on the CRT screen

This device provides visual control over the digitization of graphics data. In essence, the device consists of two digital-analog converters together with a unit linking them to the SDL. Iterative sequences of coded messages serve as input data. These are generated by the line transmitter and carry information on the co-ordinates of the illuminated dots. Any oscillographic apparatus may be used to depict the output analog signals, provided its horizontal deflection system can be governed by an external clock and the brightness of its beam can be modulated by an external signal. As the data enter the system incorporating a graphics display unit, the system controller can correct the data array appearing on the CRT and thereby alter the display dynamically.

Magnetic tape unit

The large flow of graphics data entered into the nuclear data bank and the relatively slow speed of digitization impose a specific mode of processing which may make it preferable to hold the data initially on magnetic or punched tape rather than entering them directly into the computer.

The ES-9002 standard data preparation tape drive (DPTD) was used for magnetic tape storage. This tape drive is fitted with a unit linking it to the SDC. In addition, the DPTD has been further modernized, can accommodate records of any length and can operate with the KOI-7 codes which are standard with this system. In relation to the main line, the ES-9002 can be both a receiver and a transmitter, which means that, in addition to output to a machine carrier, the reverse operation, i.e. entering data into the system, can be carried out. The structure of the SDL link unit is such that the ES-9002 DPTD's buffer can regenerate its contents onto the main line if so instructed by the controller, i.e. can thereby function as a transmitter of information to the DRGT for illumination on the CRT screen.

Connecting the graphics processing hardware to the computer

A display plugged into the computer in the standard manner and fitted with an SDL linkage unit is used to link up the system. The linkage unit comprises a multiplexer and interface circuits (Fig. 2). The codes of the symbols are transmitted to the display and passed on to the computer either from the keyboard or from the SDC depending on the position of the toggle switch on the keyboard. This solution makes it possible to dispense with special systems programs and to use the standard driver for the particular terminal.

Such visual display terminals equipped with a graphics module which allows the display of both alpha-numeric and graphical information have a much wider range of functions and a greater degree of perfection from the standpoint of graphics processing. The graphics module is constructed on a principle that is in wide use at the present time - the contents of two memories (an alpha-numeric and a graphics memory) are regenerated on the screen simultaneously. By means of a special control sequence the display switches to a graphics mode and treats the subsequent flow of data from the computer as command information with which to generate an image. As a rule, either the co-ordinates of the individual dots on the screen are transmitted or the starting and ending co-ordinates of the vectors which are to be illuminated. The microprocessor controlling the display carries out the necessary modifications and fills the graphics memory. Another control sequence is used for translation to the normal alpha-numeric mode. The working area of the graphics raster is 272 x 240 dots. The KDE 810A860 display unit serves as a source.

Special subprograms for use with the SM3 and SM4 operating systems have been developed for the benefit of users who wish to program their own graphics in high-level languages such as FORTRAN.

Available system configurations

The use of trunk-linked modules in designing the graphics processing system made it possible to set up mutually complementary systems at minimal cost. In this way, data could be entered into a nuclear physical constants base and used in various ways (off-line, on-line etc.). Figures 3 and 4 illustrate some of the more frequently encountered configurations. The systems depicted in Figs 3, 4(a) and 4(b) are the simplest and can be utilized where a computer with appropriate resources is not available in the immediate vicinity.

In cases where the quality of the input is of special importance, and primary processing is best carried out off-line (i.e. is not possible on the central computer), the configuration depicted in Fig. 3(c) should be used. For primary processing of input data, a type "Ehlektronika DZ-28" microcomputer connected to the SDL can be used. With this set-up, data obtained with the systems illustrated in Figs 3(a) and (b) can undergo primary processing. Figure 4 depicts the most suitable configuration in cases where there is direct access to the computer. With this system graphics data can be input to the computer direct without intermediate carriers, and processed on-line.

The configurations depicted in Figs 4(b) and 5 are used to enter experimental data to the base direct from the recorder. Figure 4(b) illustrates a system which enables data from the "Fialka-4M" recorder [3] to be entered to the computer via a video terminal. Two k-bytes of data can be transmitted in the space of 2 minutes to 10-15 seconds, depending on how the video terminal is connected to the computer. Figure 5 depicts an off-line system which enables the internal storage of all (max. 31) recorders to be written into standard files held on magnetic tape for subsequent computer processing. The algorithm of the control program for the system controller (an "Ehlektronika DZ-28" microcomputer) contains a number of effective design features to prevent data corruption or loss. In addition, data can also be recorded on a cassette deck which is part of the "Ehlektronika DZ-28" standard equipment.

Software resources

The software resources of the graphics data processing system comprise the following: (1) primary processing; (2) search and recording of data in the nuclear data bank; and (3) processing of data in the base. The latter two sets of programs are described in Ref. [1]. The primary processing programs include: programs to enter data with the acoustic pen and record them in the file; edit programs for these data; programs to transfer the co-ordinates to a physical system and correct various non-linear distortions along the axes of these co-ordinates; and so on. The introduction of functional keys by means of which all further processing of primary graphics data can be largely automated is a feature which makes the system particularly convenient for the evaluator. The functional keys appear on the plotting screen as squares of 1 x 1 cm, positioned somewhat to the side of the basic working image. By pressing the tip of the pen inside the square, the code of the functional key is transmitted to the output file. The following functional keys are available:

BEG - open bracket (.

END - close bracket).

LNX - open bracket for an array of dots marking the X-axis.

LNY - ditto for the Y-axis.

SCX - open bracket for an array of dots marking a scale on the X-axis.

SCY - ditto for the Y-axis.

LIN - type of scale (linear).

LOG - type of scale (logarithmic).

NLN - type of scale (non-linear).

ERX - defines the type of dot which precedes this key as the deviation (yc) along the X-axis of the dot preceding the dot "yc".

ERY - ditto for a deviation along the Y-axis.

FLG - marker key. The presence of this key permits the index of all subsequent dots to be increased by one.

CLF - flag (index) clearance.

NGR - key to reserve space for input of tabular data from a table.

NSC - the presence of this code indicates that scale data are unavailable for one of the axes used instead of SCX or SCY.

LAC - key to enter the amplitude calibration lines.

REP - marker key. Indicates that the preceding dot is for reference only.

The operations required to digitize total initial data can be described in brief as follows using Naur-Bekus's terminology:

<Operation> :: = BEG <all graphics> END

<All graphics> :: = <graphic>

<all graphics> / <graphic> NGR/

<all graphics> / NGR ... NGR

```
<Graphic>  :: = BEG <axes> <curves> END

<Curves>   :: = <curve> <curves> /

<curve> <scale> <curves>

<Curve>  :: = BEG  <information on dots>  END

<Information on dots>  :: = <dot>

<information on dots> / FLG <dot>

<information on dots> / CLF <dot>

<information on dots> / <dot> <dot>

 ERX  <information on dots> / <dot>

<dot>  ERY  <information on dots> etc.

<Axes>  : = <direction of X-axis>

<X-scale> <direction of Y-axis>

<Y-scale>  / <direction of X-axis>

 NSC  <direction of Y-axis>  <Y-scale>

<direction of X-axis> <X-scale>

<direction of Y-axis>  NSC/

<direction of X-axis>  NSC  <direction of Y-axis>  NSC

<Direction of X-axis>  :: = LNX  <all dots>  END

 Ditto for Y-axis
                      (LIN)
<X-scale>  :: = SCX   (LOG)   (all dots) END/NSC
                      (NLN)

                      (LIN)
<Y-scale>  :: = SCY   (LOG)   (all dots) END/NSC
                      (NLN)
```

Thus, processing the graphic information entered in accordance with the above protocol can be almost entirely automated, reducing manual operations to a minimum. Nuclear data evaluated by this system can be recorded and stored in an exchangeable format of the EXFOR type [4].

REFERENCES

[1] News letter of the Nea Data Bank. Nuclear Energy Agency, N 25, January, 1981.

[2] IEEE.STD 488-1975. IEEE STANDARD. Interface for Programmable Instrumentation (Hewlett-Packard Co., April 4, 1975), GOST 23131-80. Aggregated facilities for information and measurement systems. Specifications for cross-section parameters in radial and chain connection of data collection and formatting systems.

[3] GORYUSHKIN, S.I., OBSHIVALOV, V.A., ROSTOVTSEV, A.A., SHEIN, Yu.V., A device with automatic selection of the range of measurement for recording the shape of simplex signals. Pribory i tekhnika ehksperimenta (Experimental apparatus and techniques) No. 3 (1977) 121.

[4] DUNFORD, C.L., BERLAND, R.F., HUBNER, R.F., GREASY, R.J., Score II an Interactive Neutron Evaluation System (Atomics International, Canaga Park, California, March 1, 1969). AI-AEC-12757.

The article was submitted for publication on 19 January 1983.

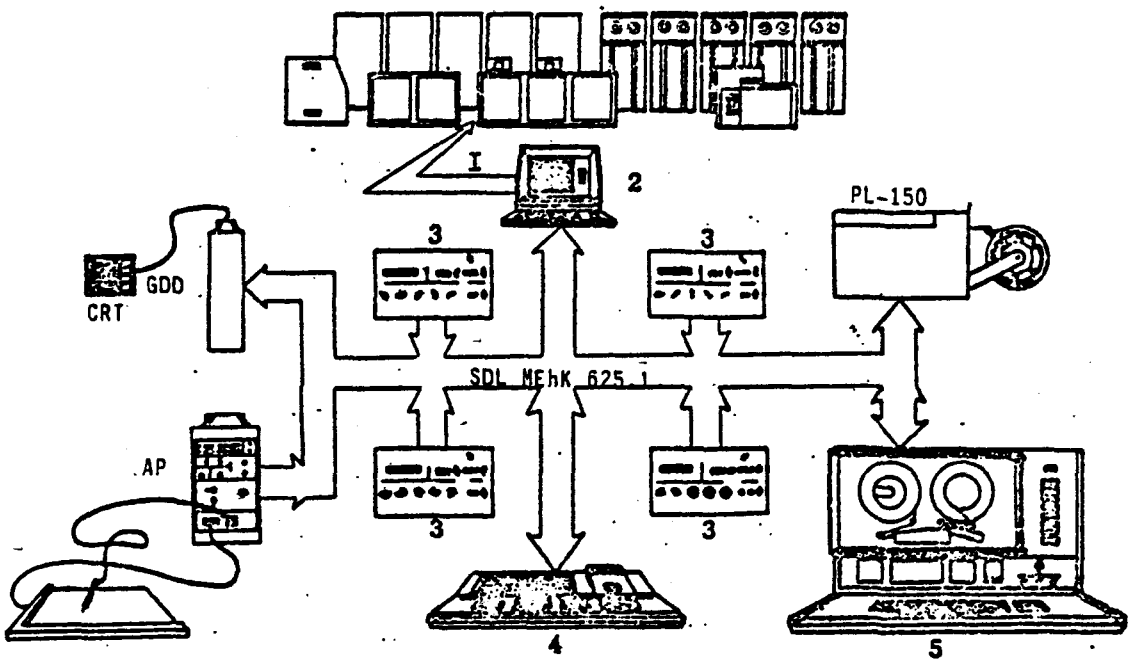

Fig. 1. Basic configuration of hardware modules: 1 - terminal channel; 2 - visual display unit with graphics option (attachment); 3 - F-4M recorder; 4 - "Ehlektronika DZ-28" microcomputer; 5 - modernized type ES-9002 DPTD.

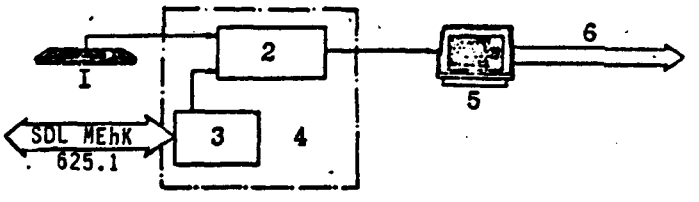

Fig. 2. Unit linking the KDE 810A860 to the SDL: 1 - keyboard; 2 - multiplexer; 3 - interface; 4 - SDL linkage unit; 5 - display; 6 - terminal channel.

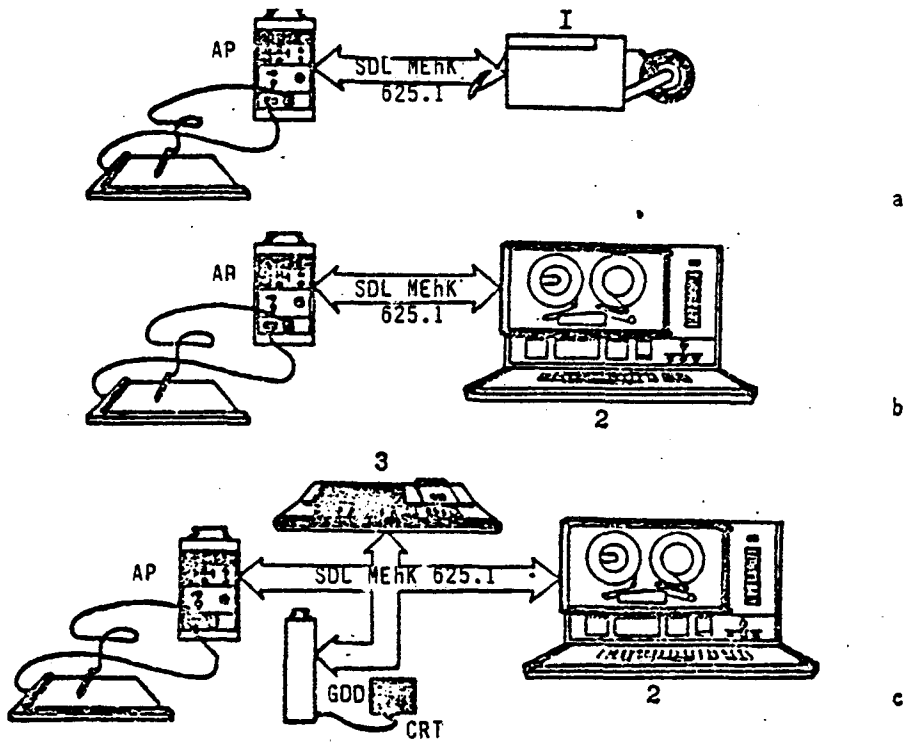

Fig. 3. Off-line graphics digitizing system with (a) paper tape; (b) magnetic tape; and (c) with visual control and edit option: 1 - PL-150 perforator; 2 - modernized type ES-9002 STPTD; 3 - "Ehlektronika DZ-28" microcomputer.

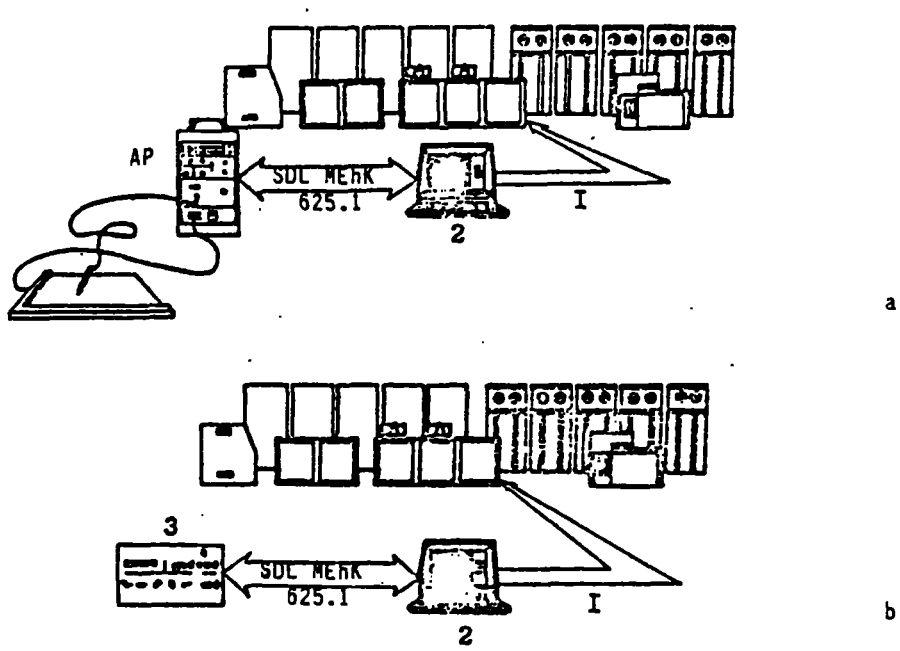

Fig. 4. System for entering graphical (a) and experimental (b) information to the computer with processing and visual control occurring simultaneously: 1 - terminal channel; 2 - type KDE 810A860 video terminal; 3 - F-4M recorder.

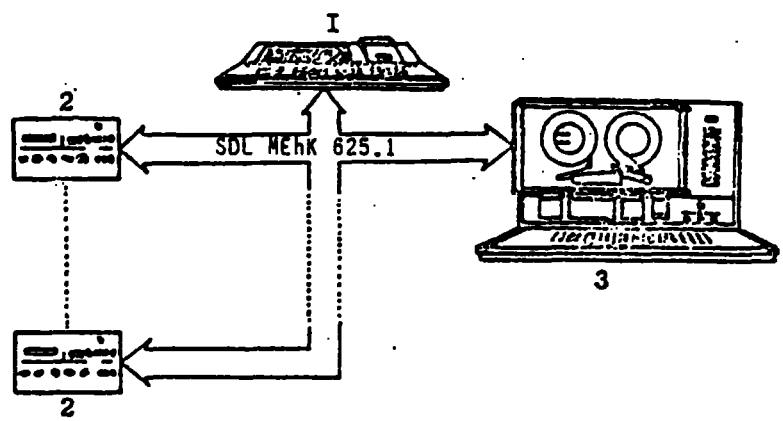

Fig. 5. Off-line system by which the contents of the memories of all recorders can be written into standard files: 1 - "Ehlektronika DZ-28" microcomputer; 2 - F-4M recorder; 3 - modernized type ES-9002 SDPTD.